J|A|C|S
ARTICLES

Published on Web 03/05/2010

Flexibility of N-Heterocyclic Carbene Ligands in Ruthenium Complexes Relevant to Olefin Metathesis and Their Impact in the First Coordination Sphere of the Metal

Francesco Ragone, Albert Poater, and Luigi Cavallo*

Dipartimento di Chimica, Università di Salerno, Via Ponte don Melillo, I-84084 Fisciano (SA), Italy

Received November 6, 2009; E-mail: lcavallo@unisa.it

Abstract: We present a detailed static and dynamics characterization of 11 N-heterocyclic carbene (NHC) ligands in Ru complexes of the general formula (NHC)Cl_2Ru=CH_2. Analysis of the dynamic trajectories indicates that the nature of the N substituent can result in extremely different flexibilities of the Ru complexes. In almost all the cases the N substituent trans to the Ru−ylidene bond is severely folded so that it protects the vacant coordination position at the Ru center. Limited flexibility is instead associated with the N substituent on the side of the Ru−ylidene bond. NHCs with a single ortho substituent, either a simple Me or a bulkier *i*-Pr group, have a preferential folding that bends the unsubstituted side of the ring toward the halide−Ru−halide plane. Analysis of the dynamics trajectories in terms of buried volume indicates that the real bulkiness of these systems can be somewhat modulated, and this flexibility is a key feature that allows NHCs to modulate their encumbrance around the metal in order to make room for bulky substrates. Analysis of the buried volume in terms of steric maps showed that NHCs with mesityl or 2,6-diisopropylphenyl N substituents have quite different reactive pockets: rather flat with constant pressure on the halide−Ru−halide plane in the former and vault-shaped with higher pressure on the sides in the latter. Regarding the NHCs with an ortho tolyl or *i*-Pr group on the N substituent, the steric maps quantify the higher impact of the unsubstituted side of the ligand in the first coordination sphere of the metal and evidence the overall C_s- and C_2-symmetric reactive pockets of the corresponding complexes. We believe that a detailed characterization of the differently shaped reactive pockets is a further conceptual tool that can be used to rationalize the experimentally different performances of catalysts bearing these ligands or to devise new applications.

Introduction

It is difficult to overemphasize the impact that N-heterocyclic carbene (NHC) ligands have had in organic and organometallic chemistry. Less than 20 years have passed since the first report of a stable NHC ligand,[1] and already catalysts containing them can be purchased in industrial scale for a number of rather different chemical transformations, such as Pd-catalyzed cross-coupling reactions of various types,[2−6] Rh- and Ir-catalyzed hydrosilylation,[6,7] C−H activation[6,8,9] and hydrogenations,[10,11] Au-catalyzed cyclization of polyunsaturated substrates,[12,13] Cu-catalyzed borylation reactions,[14,15] and finally the Ni-catalyzed dehydrogenation of ammonia−borane to H_2.[16] However, Ru-catalyzed metathesis of olefins and alkynes remains the field where the greatest impact in the forthcoming years is expected,[17−23] with applications spanning from basic transformations of raw materials in oil refinery and polymer chemistry[22,24–26] as well as from renewable resources[27,28] to sophisticated synthesis in the pharmaceutical industry.[29–31]

This impressive number of applications is possible because NHC ligands are rather flexible architectures whose stereoelec-

(1) Arduengo, A. J.; Harlow, R. L.; Kline, M. *J. Am. Chem. Soc.* **1991**, *113*, 361.
(2) Assen, E.; Kantchev, B.; O'Brien, C. J.; Organ, M. G. *Angew. Chem., Int. Ed.* **2007**, *46*, 2768.
(3) Miyaura, N.; Suzuki, A. *Chem. Rev.* **1995**, *95*, 2457.
(4) Marion, N.; Nolan, S. P. *Acc. Chem. Res.* **2008**, *41*, 1440.
(5) Würtz, S.; Glorius, F. *Acc. Chem. Res.* **2008**, *41*, 1523.
(6) Diez-Gonzalez, S.; Marion, N.; Nolan, S. P. *Chem. Rev.* **2009**, *109*, 3612.
(7) Wolfgang, A. H.; Lukas, J. G.; Christian, K.; Georg, R. J. A. *Angew. Chem., Int. Ed. Engl.* **1996**, *35*, 2805.
(8) Danopoulos, A. A.; Pugh, D.; Wright, J. A. *Angew. Chem., Int. Ed.* **2008**, *47*, 9765.
(9) Hanasaka, F.; Tanabe, Y.; Fujita, K.; Yamaguchi, R. *Organometallics* **2006**, *25*, 826.
(10) Lee, H. M.; Jiang, T.; Stevens, E. D.; Nolan, S. P. *J. Am. Chem. Soc.* **2001**, *20*, 1255.
(11) Powell, M. T.; Hou, D.-R.; Perry, M. C.; Cui, X.; Burgess, K. *J. Am. Chem. Soc.* **2001**, *123*, 8878.
(12) Nieto-Oberhuber, C.; López, S.; Jiménez-Núñez, E.; Echavarren, A. M. *Chem. Eur. J.* **2006**, *12*, 5916.
(13) Añorbe, L.; Domínguez, G.; Pérez-Castells, J. *Chem. Eur. J.* **2004**, *10*, 4938.
(14) Laitar, D. S.; Muller, P.; Sadighi, J. P. *J. Am. Chem. Soc.* **2005**, *127*, 17196.
(15) Kleeberg, C.; Dang, L.; Lin, Z.; Marder, T. B. *Angew. Chem., Int. Ed.* **2009**, *48*, 5350.
(16) Keaton, R. J.; Blacquiere, J. M.; Baker, R. T. *J. Am. Chem. Soc.* **2007**, *129*, 1844.
(17) Huang, J.; Stevens, E. D.; Nolan, S. P.; Petersen, J. L. *J. Am. Chem. Soc.* **1999**, *121*, 2674.
(18) Scholl, M.; Ding, S.; Lee, C. W.; Grubbs, R. H. *Org. Lett.* **1999**, *1*, 953.
(19) Weskamp, T.; Kohl, F. J.; Hieringer, W.; Gleich, D.; Herrmann, W. A. *Angew. Chem., Int. Ed.* **1999**, *38*, 2416.
(20) Trnka, T. M.; Grubbs, R. H. *Acc. Chem. Res.* **2000**, *34*, 18.
(21) Fürstner, A. *Angew. Chem., Int. Ed.* **2000**, *39*, 3012.
(22) Grubbs, R. H. *Handbook of Olefin Metathesis*; Wiley-VCH: Weinheim, Germany, 2003.
(23) Samojłowicz, C.; Bieniek, M.; Grela, K. *Chem. Rev.* **2009**, *109*, 3708.

tronics can be modified to a large extent, thus giving the chance for an accurate tuning of the catalytic activity. This explains why several groups have dedicated remarkable efforts to their characterization.[32−43] Focusing on the steric properties, we have developed the percent of buried volume, $\%V_{Bur}$, which is the amount of volume in the first coordination sphere of a metal occupied by a given ligand,[44] and we have used it to quantify differences between a large series of NHC ligands and even to compare them to classical phosphines.[32,35,45−47] However, all the steric analyses of NHC ligands have been performed on X-ray structures or DFT-optimized geometries and, although useful, this approach offers a somewhat limited perspective of the differences between different NHC ligands. Indeed, a series of studies clearly indicated that NHC ligands, due to an intrinsic flexibility around the N−substituent bond, are rather flexible entities and this flexibility can be exploited to achieve better or new performances in catalysis. For example, we related the efficiency in the desymmetrization of achiral trienes of the asymmetric (pre)catalyst **1** of Chart 1, developed by Grubbs,[48,49] to a peculiar folding of the NHC ligand.[50] On the basis of DFT calculations we proposed that the unsubstituted side of the NHC ligand could be bent toward the halide−Ru−halide plane, and

Chart 1

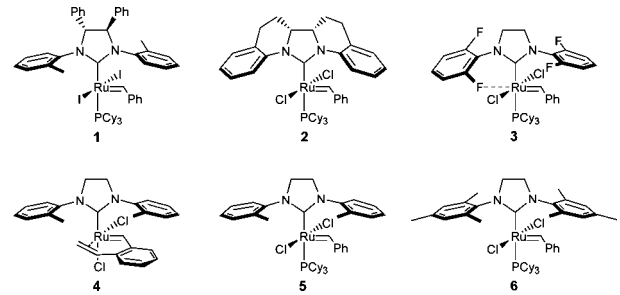

this bending is at the origin of the stereoselective ability of **1**.[50] A conceptually similar strategy was followed by Blechert, which tethered the aromatic N substituents to the bridge (see (pre-)catalyst **2** in Chart 1) to impose a folding to the N substituents with the aim of achieving high diastereoselectivity in ring rearrangement metathesis.[51] Although this strategy showed promise, **2** is of limited stability, probably due to C−H activation of the folded-down ortho C−H bond of the N substituents.

A folding of the N substituent, not imposed by features of the NHC skeleton as in **1** and **2**, was observed by Grubbs in the X-ray structure of **3** and in the NMR structure of **4**. In complex **3** the folding of the N substituent allows one of the *o*-F atoms of the NHC ligand to engage in an interaction with the Ru atom, and this interaction was hypothesized to be connected to the higher activity of **3** in a series of metathesis reactions.[52] The folding of the *N*-tolyl rings in complex **4**, instead, allows it to host the bulky C=C moiety cis to the NHC ligand.[53] Interestingly, Grubbs and Goddard proved unambiguously that the substituted side of the *o*-tolyl rings of **4** is rotated away from the bound olefin (i.e., it appears smaller to the substrate). This surprising finding led the authors to suggest that the increased reactivity and the ability to react with bulky substrates of (pre)catalysts containing *o*-tolyl rings, such as **5**, with respect to those containing the classical mesityl ring, such as **6**, could be due to an increased flexibility around the N−aromatic bond in **5** relative to **6**, which provides the substrate an increased accessibility to the metal.[53,54]

These results clearly indicate that the flexibility of NHC ligands around the N−substituent bond is a key parameter that can be used to shape appropriately the space in the first coordination sphere around the metal with practical consequences in terms of catalytic performances (both activity and selectivity). Nevertheless, no study has been focused on the characterization of this important parameter, and the scope of this paper is to fill this gap. Specifically, we will report an accurate comparative analysis of the flexibility of the NHC (pre)catalysts shown in Chart 2, as measured by the dihedral angles ϕ_1 and ϕ_2 of Chart 2, using a combined static and dynamic DFT approach integrated by an analysis of the systems based on the buried volume $\%V_{Bur}$.

(24) Mol, J. C. *J. Mol. Catal. A: Chem.* **2004**, *213*, 39.
(25) Rouhi, M. A. *Chem. Eng. News* **2002**, *80*, 29.
(26) *Ring Opening Metathesis Polymerisation And Related Chemistry*; Khosravi, E., Szymańska-Buzar, T., Eds.; Kluwer: Dordrecht, The Netherlands, 2002.
(27) Rybak, A.; Meier, M. A. R. *Green Chem.* **2007**, *9*, 1356.
(28) Malacea, R.; Fischmeister, C.; Bruneau, C.; Dubois, J. L.; Couturier, J. L.; Dixneuf, P. H. *Green Chem.* **2009**, *11*, 152.
(29) Tsantrizos, Y. S.; Ferland, J.-M.; McClory, A.; Poirier, M.; Farina, V.; Yee, N. K.; Wang, X.-j.; Haddad, N.; Wei, X.; Xu, J.; Zhang, L. *J. Organomet. Chem.* **2006**, *691*, 5163.
(30) Kanada, R. M.; Itoh, D.; Nagai, M.; Niijima, J.; Asai, N.; Mizui, Y.; Abe, S.; Kotake, Y. *Angew. Chem., Int. Ed.* **2007**, *46*, 4350.
(31) Wallace, D. J.; Goodman, J. M.; Kennedy, D. J.; Davies, A. J.; Cowden, C. J.; Ashwood, M. S.; Cottrell, I. F.; Dolling, U.-H.; Reider, P. J. *Org. Lett.* **2001**, *3*, 671.
(32) Dorta, R.; Stevens, E. D.; Scott, N. M.; Costabile, C.; Cavallo, L.; Hoff, C. D.; Nolan, S. P. *J. Am. Chem. Soc.* **2005**, *127*, 2485.
(33) de Frémont, P.; Scott, N. M.; Stevens, E. D.; Ramnial, T.; Lightbody, O. C.; Macdonald, C. L. B.; Clyburne, J. A. C.; Abernethy, C. D.; Nolan, S. P. *Organometallics* **2005**, *24*, 6301.
(34) Fantasia, S.; Petersen, J. L.; Jacobsen, H.; Cavallo, L.; Nolan, S. P. *Organometallics* **2007**, *26*, 5880.
(35) Kelly, R. A., III; Clavier, H.; Giudice, S.; Scott, N. M.; Stevens, E. D.; Bordner, J.; Samardjiev, I.; Hoff, C. D.; Cavallo, L.; Nolan, S. P. *Organometallics* **2008**, *27*, 202.
(36) Leuthäu*β*er, S.; Schmidts, V.; Thiele, C. M.; Plenio, H. *Chem. Eur. J.* **2008**, *14*, 5465.
(37) Frey, G. D.; Rentzsch, C. F.; von Preysing, D.; Scherg, T.; Muehlhofer, M.; Herdtweck, E.; Herrmann, W. A. *J. Organomet. Chem.* **2006**, *691*, 5725.
(38) Leuthäusser, S.; Schmidts, V.; Thiele, C. M.; Plenio, H. *Chem. Eur. J.* **2008**, *14*, 7195.
(39) Khramov, D. M.; Lynch, V. M.; Bielawski, C. W. *Organometallics* **2007**, *26*, 6042.
(40) Sanderson, M. D.; Kamplain, J. W.; Bielawski, C. W. *J. Am. Chem. Soc.* **2006**, *128*, 16514.
(41) Hu, X. L.; Castro-Rodriguez, I.; Olsen, K.; Meyer, K. *Organometallics* **2004**, *23*, 755.
(42) Chianese, A. R.; Kovacevic, A.; Zeglis, B. M.; Faller, J. W.; Crabtree, R. H. *Organometallics* **2004**, *23*, 2461.
(43) Chianese, A. R.; Li, X.; Janzen, M. C.; Faller, J. W.; Crabtree, R. H. *Organometallics* **2003**, *22*, 1663.
(44) Poater, A.; Cosenza, B.; Correa, A.; Giudice, S.; Ragone, F.; Scarano, V.; Cavallo, L. *Eur. J. Inorg. Chem.* **2009**, 1759.
(45) Hillier, A. C.; Sommer, W. J.; Yong, B. S.; Petersen, J. L.; Cavallo, L.; Nolan, S. P. *Organometallics* **2003**, *22*, 4322.
(46) Viciu, M. S.; Navarro, O.; Germaneau, R. F.; Kelly, R. A.; Sommer, W.; Marion, N.; Stevens, E. D.; Cavallo, L.; Nolan, S. P. *Organometallics* **2004**, *23*, 1629.
(47) Poater, A.; Ragone, F.; Giudice, S.; Costabile, C.; Dorta, R.; Nolan, S. P.; Cavallo, L. *Organometallics* **2008**, *27*, 2679.
(48) Seiders, T. J.; Ward, D. W.; Grubbs, R. H. *Org. Lett.* **2001**, *3*, 3225.
(49) Funk, T. W.; Berlin, J. M.; Grubbs, R. H. *J. Am. Chem. Soc.* **2006**, *128*, 1840.
(50) Costabile, C.; Cavallo, L. *J. Am. Chem. Soc.* **2004**, *126*, 9592.
(51) Vehlow, K.; Gessler, S.; Blechert, S. *Angew. Chem., Int. Ed.* **2007**, *46*, 8082.
(52) Ritter, T.; Day, M. W.; Grubbs, R. H. *J. Am. Chem. Soc.* **2006**, *128*, 11768.
(53) Stewart, I. C.; Benitez, D.; O'Leary, D. J.; Tkatchouk, E.; Day, M. W.; Goddard, W. A.; Grubbs, R. H. *J. Am. Chem. Soc.* **2009**, *131*, 1931.
(54) Stewart, I. C.; Ung, T.; Pletnev, A. A.; Berlin, J. M.; Grubbs, R. H.; Schrodi, Y. *Org. Lett.* **2007**, *9*, 1589.

Chart 2

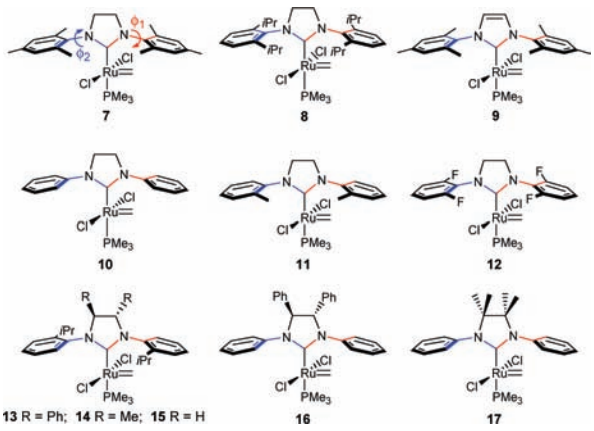

The reason to integrate standard static DFT calculations with a dynamic approach lies in the intrinsic flexible nature of the parameter under investigation. In fact, to really capture such flexibility, static DFT approaches—or analysis of X-ray structures—are poorly effective, since they freeze the system into a minimum of the potential energy surface. A dynamic approach, instead, is better suited, since it allows the real dynamic behavior of the system with time to be followed and the ensemble of accessible conformations to be explored. This is a relevant issue, since the work of Grubbs and Goddard has clearly indicated that NHC ligands respond actively to the steric requirements of an incoming ligand by adopting conformations that minimize their steric bulkiness in the first coordination sphere of the metal.

Computational Details

Static Calculations. The DFT static calculations were performed at the GGA level with the Gaussian03 package,[55] using the BP86 functional of Becke and Perdew.[56−58] The electronic configuration of the molecular systems was described with the standard split-valence basis set with a polarization function of Ahlrichs and co-workers for H, C, N, O, P, F, and Cl (SVP keyword in Gaussian03),[59] For Ru we used the small-core, quasi-relativistic Stuttgart/Dresden effective core potential, with an associated (8s7p6d)/[6s5p3d] valence basis set contracted according to a (311111/22111/411) scheme (standard SDD keywords in Gaussian03).[60] The geometry optimizations were performed without symmetry constraints, and the characterization of the located stationary points was performed by analytical frequency calculations. Solvent effects, including contributions of nonelectrostatic terms, have been estimated in single-point calculations on the gas-phase optimized structures, based on the polarizable continuum solvation model PCM, using CH_2Cl_2 as the solvent.[61]

Dynamic Calculations. The dynamics DFT simulations were performed using the Born−Oppenheimer scheme as implemented in the CP2K Quickstep code.[62] The electronic structure calculations were done at the DFT level using the Perdew−Burke−Ernzerhof exchange and correlation functional.[63] Within CP2K the Kohn−Sham molecular orbitals are described by a linear combination of Gaussian-type orbitals, whereas an auxiliary planewave basis set is employed in order to expand the electron density.[64] A double-ζ basis set with a polarization function, in conjunction with the Goedecker−Teter−Hutter pseudopotentials, was used for all the atoms (standard DZVP-GTH keywords in CP2K).[65] The auxiliary planewave basis set was defined by a cubic box of 20 × 20 × 20 Å^3 and by an energy cutoff of 300 Ry. The equations of motion were integrated using a time step of 0.5 fs. The systems were first equilibrated at 300 K for 2 ps in the NVT ensemble and then were sampled for an additional 10 ps.

Table 1. Minimized Values of the ϕ_1 and ϕ_2 Angles in Systems **7**−**17**, the Gas-Phase Energies, in kcal/mol, of the Same Systems in a Geometry in Which the ϕ_1 and/or ϕ_2 Angles Are Forced To Be Equal to 90°,[a] and $\%V_{Bur}$ Values

system	ϕ_1	ϕ_2	E (ϕ_1 = 90°)	E (ϕ_2 = 90°)	E (ϕ_1 = ϕ_2 = 90°)	$\%V_{Bur}$
7	91.0	92.2	0.0 (0.0)	0.0 (0.0)	0.0 (0.0)	31.6
8	88.9	93.6	0.0 (0.0)	0.0 (0.1)	0.0 (0.1)	31.9
9	91.5	92.4	0.0 (0.0)	0.0 (0.0)	0.0 (0.0)	30.9
10	134.7	27.0	1.3 (0.1)	2.5 (2.8)	3.4 (3.4)	32.6
11	92.3	113.7	0.0 (0.0)	0.8 (0.7)	0.7 (0.5)	30.6
12	78.0	44.8	0.1 (0.1)	0.9 (0.5)	1.0 (0.6)	34.1
13	66.3	59.0	1.4 (1.4)	2.2 (2.3)	3.9 (3.8)	31.2
14	66.1	60.5	1.0 (0.9)	1.5 (1.6)	2.5 (2.5)	30.8
15	64.2	57.8	1.2 (1.2)	1.9 (2.2)	3.0 (3.0)	30.3
16	66.0	158.5	0.4 (0.1)	2.2 (2.2)	2.7 (2.6)	32.4
17	66.6	69.5	0.2 (0.0)	0.3 (0.3)	0.6 (0.6)	30.4

[a] Values in parentheses are the energy differences in CH_2Cl_2.

As a warning to the reader, we note here the two main approximations of our dynamic simulations. First, it is difficult to understand if they are long enough to achieve a well-converged sampling, particularly for the most flexible systems. Nevertheless, analysis of a symmetric ruthenacyclobutane system, where the ϕ_1 and ϕ_2 angles are not distinguishable, indicated that the ϕ_1 and ϕ_2 distributions overlap nicely (see the Supporting Information). This indicates that 10 ps sampling is enough to capture properly the flexibility around ϕ_1 and ϕ_2. Second, we simulated the systems in the gas phase, while they are usually used in rather polar solvents such as CH_2Cl_2. However, due to the extreme computational cost of these simulations for longer sampling the inclusion of explicit solvent molecules, even by QM/MM techniques, still is very expensive. Nevertheless, considering that we worked on related systems, these approximations should affect all the systems similarly. Further, the main aim of this work is to provide differences and trends among systems, rather than providing exact and accurate values for some parameters. Therefore, we believe that the aforementioned approximations have a minor impact on the trends we obtained.

$\%V_{Bur}$ Calculations. The buried volume calculations were performed with the Samb*V*ca. package developed by us.[44] The radius of the sphere around the metal center was set to 3.5 Å, while for the atoms we adopted the Bondi radii scaled by 1.17, and a mesh of 0.1 Å was used to scan the sphere for buried voxels. The steric maps were evaluated with a development version of the Samb*V*ca. package.

Results and Discussion

Static Analysis. We start this part discussing the ϕ_1 and ϕ_2 values in the structure of complexes **7**−**17** as obtained from a standard geometry optimization. The optimized values are reported in Table 1. We first note that the optimized ϕ_1 and ϕ_2 values of system **7**, bearing the SIMes NHC ligand, are practically equal to 90°, which means that the mesityl rings are

(55) Frisch, M. J.; et al. *Gaussian03*, revision E.01; Gaussian Inc., Wallingford, CT, 2003.
(56) Becke, A. D. *Phys. Rev. A* **1988**, *38*, 3098.
(57) Perdew, J. P. *Phys. Rev. B* **1986**, *33*, 8822.
(58) Perdew, J. P. *Phys. Rev. B* **1986**, *34*, 7406.
(59) Schaefer, A.; Horn, H.; Ahlrichs, R. *J. Chem. Phys.* **1992**, *97*, 2571.
(60) Kuechle, W.; Dolg, M.; Stoll, H.; Preuss, H. *J. Chem. Phys.* **1994**, *100*, 7535.
(61) Tomasi, J.; Persico, M. *Chem. Rev.* **1994**, *94*, 2027.
(62) VandeVondele, J.; Krack, M.; Mohamed, F.; Parrinello, M.; Chassaing, T.; Hutter, J. *Comput. Phys. Commun.* **2005**, *167*, 103.
(63) Perdew, J. P.; Burke, K.; Ernzerhof, M. *Phys. Rev. Lett.* **1996**, *77*, 3865.
(64) Lippert, G.; Hutter, J.; Parrinello, M. *Mol. Phys.* **1997**, *92*, 477.
(65) Goedecker, S.; Teter, M.; Hutter, J. *Phys. Rev. B* **1996**, *54*, 1703.

perpendicular to the NHC plane. The same occurs for systems **8** and **9**, bearing the SIPr and IMes NHC ligands, respectively. Of course, freezing the ϕ_1 and ϕ_2 angles to exactly 90° for **7**−**9** has no energy consequences. However, the ϕ_1 and ϕ_2 angles in the unsubstituted system **10**, bearing the SIPh NHC ligand, strongly deviate from 90° with the ϕ_2 angle more coplanar with the NHC ring rather than orthogonal to it. This is a clear consequence of the space available around the vacant coordination position trans to the Ru−ylidene bond, which allows the phenyl N substituent to rotate remarkably. Of course, this rotation is prodrome to deactivation reactions through activation of the ortho C−H bonds, since they place the ortho H atom close to the ylidene moiety.[51,66,67] Forcing either ϕ_1 or ϕ_2 to be equal to 90° results in structures which are 1.3 and 2.5 kcal/mol higher in energy, respectively, which indicates that the phenyl ring can rotate almost freely. Further, fixing both ϕ_1 and ϕ_2 at 90° results in a structure that is 3.4 kcal/mol higher in energy, which indicates that rotations around ϕ_1 and ϕ_2 are not connected.

Two Ph substituents on the C4 and C5 atoms of the NHC skeleton, as in system **16**, do not prevent rotation around the N−substituent bonds very effectively (see the quite large deviation of the optimized ϕ_1 and ϕ_2 values for **16**), while a better control of these angles is obtained with four Me substituents on the NHC skeleton (see system **17**). Remarkably, the *o*-tolyl system **11**, bearing the SITol NHC ligand, presents ϕ_1 very close to 90° and ϕ_2 deviating from it by roughly 20° only. This clearly indicates that one single Me ortho substituent is already enough to prevent rotation of the N substituents, even on the side of the vacant coordination position trans to the Ru−ylidene bond. Nevertheless, as shown by Grubbs and Goddard, the NHC of **11** is flexible and is able to rotate away from ϕ_1 and ϕ_2 ∼90° when a bulky substrate coordinates to the metal.[53,68] This underlines the need for a method able to describe properly the flexibility of these complexes.

The optimized *o*-F substituted system **12** presents two rather different structures which are quite close in energy. The most stable, reported in Table 1, is characterized by a ϕ_2 angle deviating remarkably by 90°, which allows for the establishment of a Ru···F interaction as observed in the X-ray structure.[69] However, we also localized a structure with both ϕ_1 and ϕ_2 very close to 90° and thus with no Ru···F interaction, which is only 0.5 kcal/mol higher in energy.

Moving to the asymmetric systems **13**−**15**, we note that these systems present nearly identical ϕ_1 and ϕ_2 values, deviating by roughly 20−30° from 90°, even in the absence of any substituent on the NHC skeleton. This deviation, which is in line with the X-ray structure of a complex strictly related to **13**,[48] indicates that the folding of the N substituents in **13**−**15** is dictated by steric repulsion between the *i*-Pr substituents and the halides, rather than by repulsion between the *i*-Pr substituents and the substituents on the NHC skeleton. Surprisingly, freezing ϕ_1 or ϕ_2 to 90° costs no more than 2.5 kcal/mol, which indicates that some flexibility around the N−substituent bond is possible also for these systems. Again, the energy of the structure with both ϕ_1 and ϕ_2 fixed to 90° indicates that no correlation between the two angles exists.

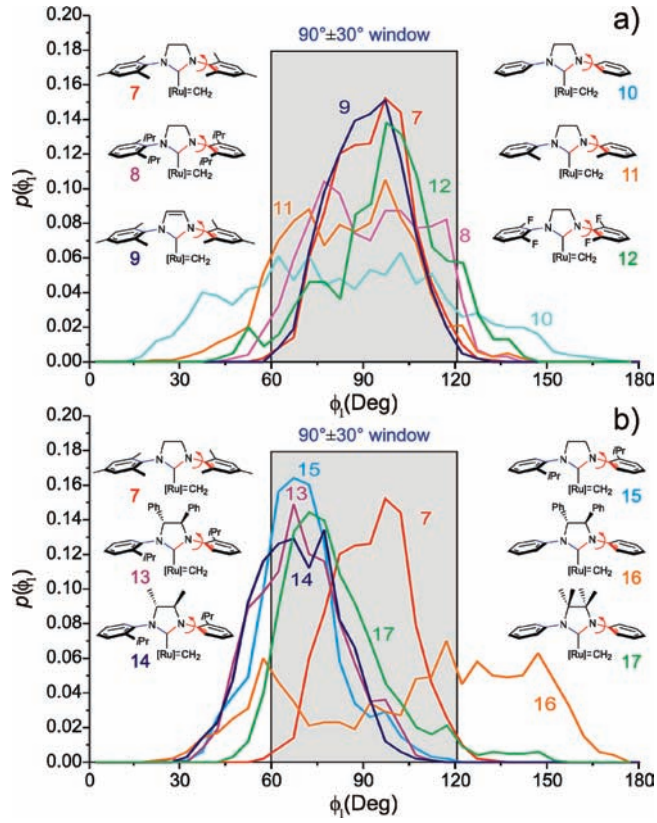

Figure 1. Distribution of the ϕ_1 angle for systems **7**−**17**. [Ru] stands for the $Ru(Cl_2)(PMe_3)$ moiety. $\phi_1 = 90$ or −90° corresponds to geometries with the aromatic ring of the N substituent perpendicular to the mean plane of the NHC ring, while $\phi_1 = 0$ or 180° corresponds to geometries with the aromatic ring of the N substituent coplanar with the mean plane of the NHC ring.

Dynamics Analysis. In this section we report on molecular dynamics simulations we performed to get insights on the flexibility of **7**−**17**. The distribution of the ϕ_1 angle for systems **7**−**17**, as obtained by the statistical analysis of the 10 ps molecular dynamics trajectories, is reported in Figure 1. For the sake of clarity, the distributions of systems **7**−**12**, which correspond to systems where the interest is focused on the nature of the N substituent, are reported in Figure 1a, while those of systems **13**−**17**, which are systems that allow us to investigate the effect of substituents on the C−C bridge of the NHC ring, are reported in Figure 1b. In both cases system **7** is used as reference. Consistently with the static calculations, the ϕ_1 distribution of **7** shows a peak centered at 90°, and the flexibility is substantially restricted to ±15°. The unsaturated analogous IMes system **9** shows an almost overlapping distribution, indicating that the nature of the NHC skeleton has a limited impact on the flexibility of the ϕ_1 angle. Conversely, the SIPr-based system **8** shows a flatter and somewhat broader and jagged peak, which is due to the bumping of the *i*-Pr substituents into the halide ligands, which causes the ϕ_1 angle to oscillate wildly in the 60−120° window. This result indicates that the static calculations offer a limited perspective only. Also unexpected and quite instructive is the behavior of the *N*-phenyl system **10**, with a rather broad ϕ_1 distribution covering the range 30−150° and tails almost approaching $\phi_1 = 0$ or 180°, which correspond to geometries with the phenyl ring almost coplanar with the NHC mean plane. Of course, conformations with $\phi_1 \approx 0$ or 180° are geometrically very suited to interact with the ylidene moiety in a C−H (de)activation reaction.[51,66,67]

(66) Mathew, J.; Koga, N.; Suresh, C. H. *Organometallics* **2008**, *27*, 4666.
(67) Poater, A.; Cavallo, L. *J. Mol. Catal. A: Chem.* [Online early access]. DOI: 10.1016/j.molcata.2010.02.023. Published Online: Feb 21, 2010.
(68) Benitez, D.; Tkatchouk, E.; Goddard, W. A. *Organometallics* **2009**, *28*, 2643.
(69) Vougioukalakis, G. C.; Grubbs, R. H. *Organometallics* **2007**, *26*, 2469.

At this point we can turn our attention to the *o*-tolyl system **11**, which in principle should have a behavior intermediate between those of **7** and **10**. Instead, the ϕ_1 distribution of **11** is quite peaked, which means that a single Me group on the N substituent is enough to reduce remarkably the flexibility of this system. Furthermore, the distribution of **11** almost overlaps with that of **7** at higher ϕ_1 values, which indicates that the folding of the substituted side of the *o*-tolyl ring toward the Cl−Ru−Cl plane is controlled by interactions between the ortho substituent and the nearby Cl atom. Conversely, the distribution of **11** presents a substantially larger shoulder at low ϕ_1 values, which indicates that the *o*-tolyl ring can fold more the unsubstituted side toward the Cl−Ru−Cl plane, and this rotation is only hindered by the bumping of the *o*-Me group of the tolyl ring into the $-CH_2CH_2-$ bridge of the imidazoline ring. This result relates well with the good catalytic performances of **11**, since it is a less hindered catalyst than **7**, but the limited flexibility with respect to **10** prevents it from suffering C−H deactivation reactions. The *o*-F system **12** presents a somewhat narrower peak with a shoulder at higher ϕ_1 values, indicating that the F atoms are large enough to prevent almost free rotation as in **10**, but they are smaller than a Me group, as in **7**, so that some folding can occur. No clear evidence of a Ru···F interaction was observed during the dynamics, although the most stable CP2K optimized structure of **12** presents this interaction, and it is 1.8 kcal/mol more stable than the CP2K optimized structure with both ϕ_1 and ϕ_2 being ca. 90° (see also the above discussion in Static Analysis). Indeed, the Ru···F interaction is lost as the dynamics of **12** is started, indicating that the small energy preference for the structure with this interaction in place is not strong enough to preserve it under dynamic conditions. This suggests that under catalytic conditions this interaction is probably not very relevant.

We move now to the systems which present some degree of substitution on the $-CH_2CH_2-$ bridge of the imidazoline ring. The three systems with a single ortho *i*-Pr group, systems **13**−**15**, present a similarly shaped peak roughly centered at 70°, in agreement with the static geometry optimization discussed before, and with the crystallographic structure of a strictly related compound.[48] This indicates that on moving from a single *o*-Me group (system **11**) to a single *o*-*i*-Pr group (system **15**) there is a remarkable change in the flexibility of the ϕ_1 angle. In fact, the shoulder at low ϕ_1 values of **11** is increased into a peak, while conformations at $\phi_1 > 90°$ are simply not accessible. The similar behavior of **13**−**15** indicates that this substantial change is not related to the presence of substituents on the NHC bridge and confirms that the driving force that pushes the substituted side of the N-aromatic ligand of **13** and **14** away from the Cl−Ru−Cl plane is the interaction of the *i*-Pr group with the halide ligands.

We compare now **16** and **17** to **10**. The distribution of **16** is rather flat, as is that of **10**, but presents a low and broad peak at ϕ_1 values around 120−150°. This folds the *N*-phenyl ring toward the phenyl ring on the NHC bridge, to engage in a sort of van der Waals stacking interaction. However, **17** shows a rather sharp peak. This indicates that the four Me groups on the NHC bridge, besides placing the phenyl N substituent perpendicular to the NHC ring, restrict remarkably the conformational freedom of the ϕ_1 angle. This reinforces the conclusion that the high stability of **17** can be ascribed to the difficulty of the ortho C−H bonds of the phenyl rings to undergo C−H (de)activation reactions.

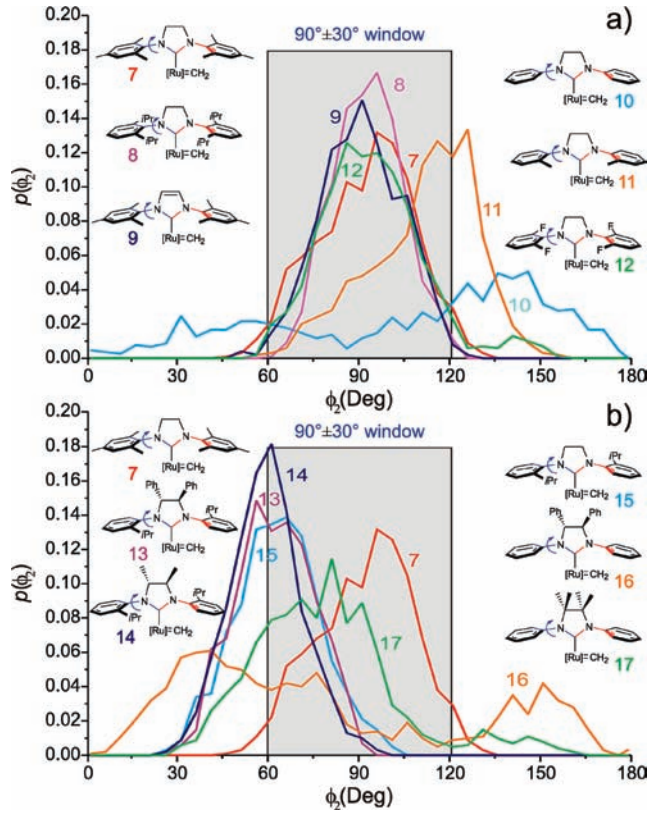

Figure 2. Distribution of the ϕ_2 angle for systems **7**−**17**. [Ru] stands for the $Ru(Cl_2)(PMe_3)$ moiety. $\phi_2 = 90$ or $-90°$ corresponds to geometries with the aromatic ring of the N substituent perpendicular to the mean plane of the NHC ring, while $\phi_2 = 0$ or 180° corresponds to geometries with the aromatic ring of the N substituent coplanar with the mean plane of the NHC ring.

We discuss now the ϕ_2 angle, which is the angle around the N−substituent bond opposite to the Ru−methylidene bond (see Figure 2). For **7**−**12**, the ϕ_2 plots show rather broad and overlapping peaks centered around 90° with the only noticeable exceptions of **10** and **11**. The former presents a very flat ϕ_2 profile, indicating that this phenyl group rotates almost freely. This is different from the phenyl on the side of the Ru−methylidene bond, where the methylidene group prevented free rotation. System **11**, instead, presents a well-shaped ϕ_2 peak shifted roughly 30° from that of **7**−**9**. This indicates that the corresponding *o*-tolyl ring assumes a preferential conformation that, again, folds the methyl-substituted side away from the Cl−Ru−Cl plane. System **12** presents a ϕ_2 peak rather similar to that of **7**, which means that the corresponding F-substituted ring, consistent with the static calculations, has no tendency to rotate and engage with the metal in a Ru···F interaction. Moving to **13**−**17** (see Figure 2b), we note that **13**−**15** present almost overlapping peaks clearly shifted from 90°. This indicates once more that the presence of substituents on the C4 and C5 atoms of the imidazoline skeleton has no influence on the conformational freedom of the N substituents, which is instead completely dictated by the single ortho *i*-Pr group. Further support is given by **16**, where the Ph substituents on the imidazoline skeleton are substantially unable to lock rotation of the phenyl ring around the ϕ_2 bond. Again, this rotational freedom can be restrained by complete substitution of the imidazoline skeleton, such as in **17**, which presents a peak rather similar to that of **7**.

Finally, we also investigated the behavior of the ϕ_1 and ϕ_2 dihedral angles in the key species of the metathesis reaction,

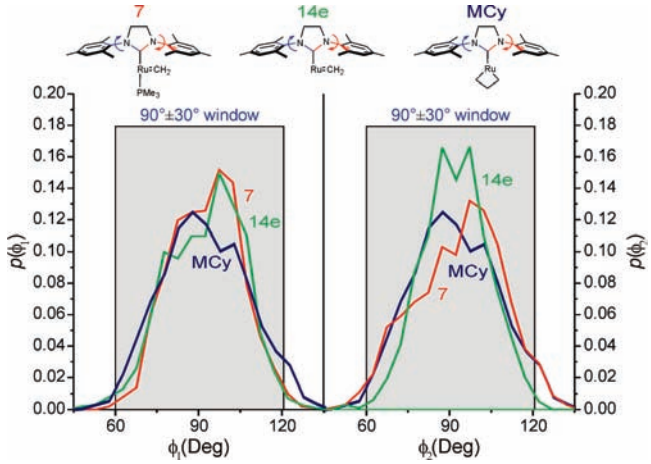

Figure 3. Distribution of the ϕ_1 and ϕ_2 angles for the (pre)catalyst, the 14e intermediate, and the metallacycle of system **7**.

which are the 14e complex from dissociation of the PMe_3 moiety from **7** and the ethene-coordinated and metallacyclic intermediates. However, the ethene-coordinated intermediate is not stable enough under our simulation conditions and very rapidly collapses into the metallacyclic intermediate. This behavior is consistent with the known very low barrier for the metathesis step calculated by several authors.[70−73] For this reason, we restricted the analysis to the 14e and to the metallacyclic intermediates, and again we compared them with the starting (pre)catalysts **7** (see Figure 3). The distribution of the ϕ_1 angle in the two intermediates strongly resembles that in the (pre-)catalyst **7**, although that corresponding to the metallacycle is slightly less peaked. Similar small differences are calculated for the distributions of the ϕ_2 angle of **7** and of the metallacycle, while that corresponding to the 14e intermediate is slightly more peaked. However, the general conclusion is that the ϕ_1 and ϕ_2 distributions are rather similar in the three key species of olefin metathesis, which is consistent with the previous analysis which suggested the main role of the halide ligands and of the ylidene moiety in determining the flexibility of the N substituents of the NHC ligand.

Buried Volume Analysis. In the previous sections we shed light on the different flexibility showed by **7**−**17**. However, the analysis did not quantify the impact that these differences have in the first coordination sphere of the metal, where reactivity occurs. To clarify this point we use the $\%V_{Bur}$ descriptor.[32,44,45,74,75] The $\%V_{Bur}$ values of the NHC ligands in the optimized structures of **7**−**17** are reported in Table 1. In line with our analysis of $\%V_{Bur}$ in the model $(NHC)Ir(CO)_2Cl$ systems,[44] the SIMes ligand has a $\%V_{Bur}$ value slightly greater than that of the corresponding unsaturated IMes ligand. This is a consequence of the different nature of the NHC skeleton,which results in the N−C−N angle being 3.8° greater in the saturated imidazoline ring of the SIMes ligand than in the unsaturated imidazole ring of the IMes ligand (108.0 and 104.2° in SIMes and IMes, respectively).[76] This subtle geometrical difference bends the N substituent of the saturated NHCs slightly more toward the metal (see the shorter Ru−C_{ipso} distances in Scheme 1), thus increasing the steric demand measured by the $\%V_{Bur}$.

Scheme 1

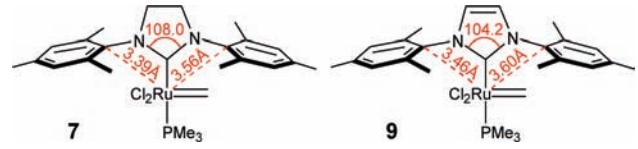

In addition to these two reference systems, we note that the SIPh ligand of **10** shows a $\%V_{Bur}$ value of 32.6, which is greater than that of the SIMes- and SIPr-based systems **7** and **8**. This can be related to the remarkable rotation of the N substituents that places the phenyl groups almost coplanar to the NHC mean plane. Similar behavior is shown by **16**, consistent with the high folding around ϕ_1 and ϕ_2. However, the tetrasubstituted NHC of **17** shows a $\%V_{Bur}$ value of only 30.4, indicating once more the role of the four Me groups on the C4 and C5 substituents of the NHC ring in keeping the N substituent perpendicular to the NHC ring. Thus, our analysis is in line with the strategy designed by Grubbs and co-workers to achieve good catalytic performances in the ring-closing metathesis of tetrasubstituted olefins: a small N substituent to accommodate large substrates and a bulky backbone to prevent its rotation, which would reduce stability.[77] Differently from the results on the model $(NHC)Ir(CO)_2Cl$ systems, the SIPr ligand of **8** has a $\%V_{Bur}$ value slightly larger than that of the SIMes ligand of **7**, although it presents remarkably bulkier *i*-Pr ortho substituents. With regard to the NHCs with a single ortho substituent, the ITol NHC of **11** shows a $\%V_{Bur}$ value slightly smaller than that of the SIMes in **7** and of the NHC of **13**. This last result is clearly a consequence of the folding of the *i*-Pr substituents away from the halide−Ru−halide plane.

However, the $\%V_{Bur}$ analysis based on static structures does not reflect the flexibility exhibited by the NHC ligands during the molecular dynamics simulations discussed above and highlighted by Grubbs and Goddard.[53] To investigate this point, we have analyzed in terms of the $\%V_{Bur}$ the dynamic trajectories of the most relevant among the systems of Chart 2, namely, **7**−**9** and **11**, to investigate the effect of the N substituent, and **10**, **13**, and **17**, to investigate the effect of substituents on the NHC C4−C5 bridge. The distribution of the $\%V_{Bur}$ of the corresponding NHCs, calculated on the structures collected during the molecular dynamics simulations, are reported in Figure 4.

Starting from **7**, it is clear that the $\%V_{Bur}$ obtained from the geometry optimization only corresponds to the peak of a fairly broad distribution. The $\%V_{Bur}$ of the SIMes in **7** spans easily over the 30−34% range, and the distribution overlaps with those of the other systems. This result gives a completely different perspective of the impact that the SIMes ligand has in the first coordination sphere around the metal and clearly indicates that even small variations in the geometry of the rather rigid SIMes ligand can have a strong impact in terms of bulkiness.

The $\%V_{Bur}$ distribution of the SIPr in **8** is peaked at higher values and is somewhat broader than that of the SIMes in **7**. It also presents a rather long tail at high values, evidencing again

(70) Cavallo, L. *J. Am. Chem. Soc.* **2002**, *124*, 8965.
(71) Adlhart, C.; Hinderling, C.; Baumann, H.; Chen, P. *J. Am. Chem. Soc.* **2000**, *122*, 8204.
(72) Vyboishchikov, S. F.; Bühl, M.; Thiel, W. *Chem. Eur. J.* **2002**, *8*, 3962.
(73) Benitez, D.; Tkatchouk, E.; Goddard, W. A. I. *Chem. Commun.* **2008**, 6194.
(74) Correa, A.; Cavallo, L. *J. Am. Chem. Soc.* **2006**, *128*, 13352.
(75) Cavallo, L.; Correa, A.; Costabile, C.; Jacobsen, H. *J. Organomet. Chem.* **2005**, *690*, 5407.
(76) Magill, A. M.; Cavell, K. J.; Yates, B. F. *J. Am. Chem. Soc.* **2004**, *126*, 8717.
(77) Chung, C. K.; Grubbs, R. H. *Org. Lett.* **2008**, *10*, 2693.

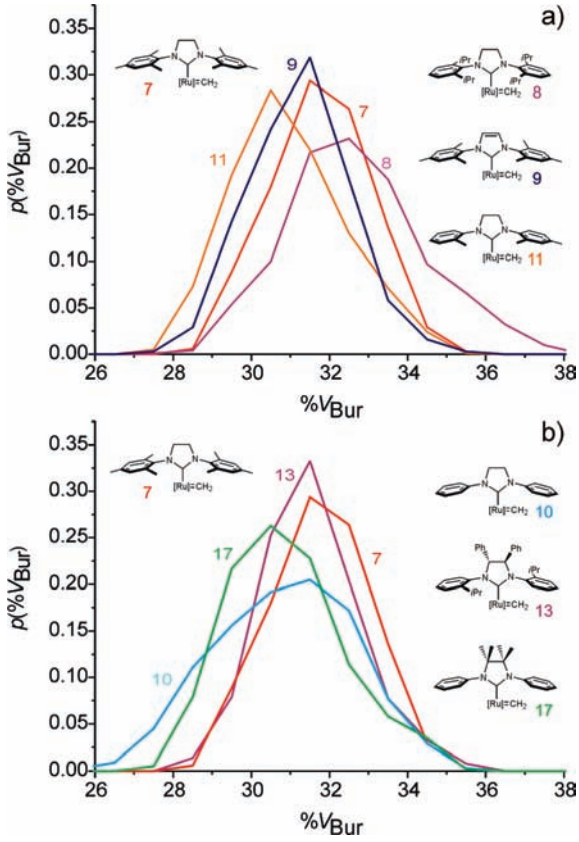

Figure 4. Distribution of the $\%V_{Bur}$ for selected systems.

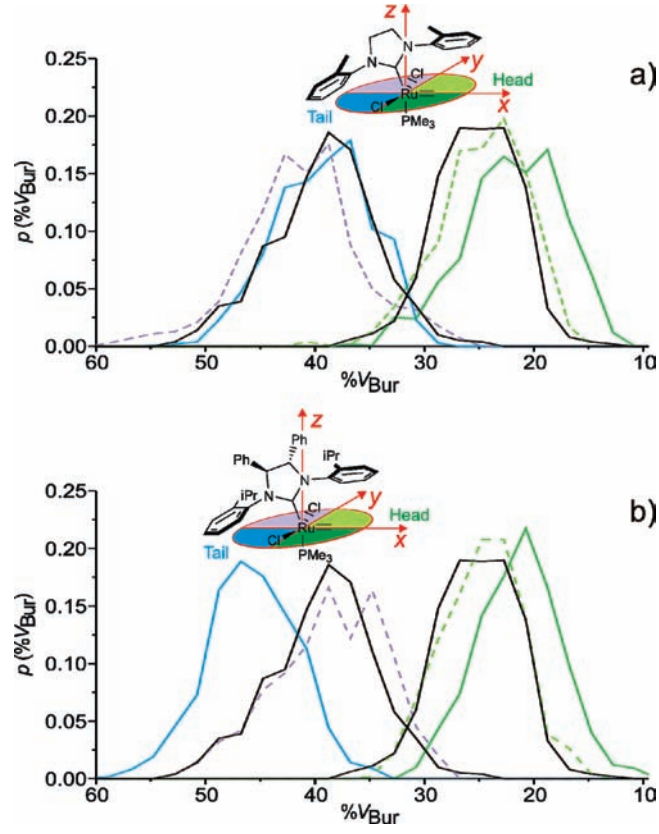

Figure 5. Distribution of the $\%V_{Bur}$ values in the quadrants around the metal center for selected systems.

that normal vibrations of the SIPr ligand, not captured by static methods, have a strong influence on the amount of space this bulky ligand requires. The distribution of the unsaturated IMes in **9** is shifted at slightly smaller values, consistent with previous analysis, suggesting that the unsaturated NHCs are slightly less bulky than the saturated counterparts. As concerns the *o*-tolyl NHC in **11**, the distribution is slightly broader and it is peaked at lower values relative to the SIMes in **7**, highlighting that the single methyl substitution of the *o*-tolyl N substituent has a doubly positive effect. It results in a less demanding ligand so that **8** can accommodate bulky substrates better than **7**,[53] but it is bulky enough to prevent large rotations around the N−substituent bonds, thus decreasing the rate of deactivation reactions.

Moving to the NHC in **13** and **17**, the single *i*-Pr ligand of **13** results in a bulkiness substantially similar to that of the SIMes in **7**, with the distribution shifted to slightly lower $\%V_{Bur}$ values, although the complete picture is much more complicated (see below). Very instructive is instead the comparison between the unsubstituted NHC of **10** and the tetramethyl-substituted NHC of **17**. The former presents a very broad peak, consistent with the high conformational freedom around the N−substituent bonds, and the latter presents a much narrower distribution. In a sense, the tetramethyl substitution confers to **17** a better defined structure, which is a concept that could be useful in the rational design of new ligands with a controlled behavior.

We now proceed to dissect the $\%V_{Bur}$ values of some of the most interesting NHCs in terms of quadrant contributions. In a previous paper,[50] we proposed that the stereoselectivity of **13** could be explained by considering that the folding of the aryl N substituents could result in a different space occupation of the quadrants around the metal center. The $\%V_{Bur}$ value allows this difference to be measured. The distributions of $\%V_{Bur}$ in the four quadrants are reported in Figure 5 for the representative NHCs of **11** and **13** and, for comparison, for the parent SIMes NHC of **7**. Due to the symmetry of the SIMes ligand the two head quadrants (as well as the two tail quadrants) present identical $\%V_{Bur}$ distributions, and thus we only report the averages (black lines in Figure 5). The tail quadrants are much more buried by the SIMes ligand than the head quadrants, average $\%V_{Bur}$ values peaking at roughly 38% and 25%, respectively. This is a clear consequence of the vacant coordination position trans to the Ru−methylidene bond, which allows the NHC ligand to fold back in order to minimize steric interactions with the methylidene group (the C(NHC)−Ru=CH_2 angle in **7** is 103.8°).

Focusing on the NHC of **11**, the asymmetry of the *o*-tolyl N substituents splits the $\%V_{Bur}$ peaks (colored lines in Figure 5). As a result the peaks corresponding to the substituted side of the *o*-tolyl rings (pale-colored quadrants and dashed lines in Figure 5) are shifted to lower values, which means that these quadrants are less encumbered by the NHC ligand and thus are more accessible to bulky substrates. The splitting on both the tail and the head side is roughly 3−4%, illuminating how small structural differences can have an impact on catalytic performances. Interestingly, on the head side the $\%V_{Bur}$ distribution of the unsubstituted part of the *o*-tolyl ring almost overlaps that of IMes, a consequence of the increased rotation around the ϕ_1 angle. This suggests that similar bulkiness can be obtained by playing with conformational effects (rotation around ϕ_1) rather than substitution effects (adding a Me group in the ortho position).

Moving to the asymmetric NHC of **13**, an even more pronounced splitting of the distributions in the head and tail quadrants is observed. Also in this case the less hindered

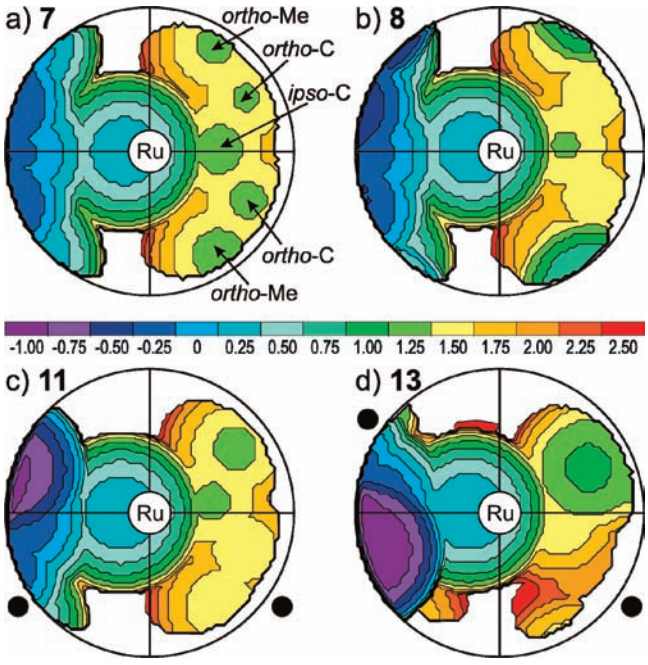

Figure 6. $\%V_{Bur}$ maps of the NHC in the optimized geometries of (a) **7**, (b) **8**, (c) **11**, and (d) **13**. The spots corresponding to the ortho and ipso C atoms of the mesityl ring and of the *o*-methyl substituents of **7** are indicated by arrows. The quadrants occupied by the *o*-methyl and *o*-isopropyl substituents in **11** and **13** are indicated by a black dot. The coloring scale of the isocontour levels, in Å, is also reported.

quadrants correspond to the *i*-Pr substituted side of the NHC, which is a strong support to the mechanism of stereoselectivity we proposed.[50] Interestingly, the splitting of the $\%V_{Bur}$ distributions in the tail quadrants is remarkably high, more than 10%, consistent with a severe folding of the N substituent on the side of the vacant coordination position at the Ru center.

We enter now into the first coordination sphere of the metal through the steric maps shown in Figure 6 for selected systems. The reason for this choice is that the $\%V_{Bur}$ descriptor—like the Tolman cone angle[78]—measures an average property, while catalysis can be determined by a different distribution of the buried volume in the first coordination sphere of the metal. The steric maps of Figure 6 report the value along the *z* axis at which the NHC ligand starts to bury space in the coordination sphere around the Ru center. Positive values of the isocontour lines refer to the top half-sphere, which is the half-sphere where the NHC ligand dwells. The geometries analyzed are the optimized geometries of Table 1 and have been aligned as shown in Figure 5.

Focusing on the SIMes in **7**, the tail mesityl group shields the vacant coordination position on the Ru center (see the deep blue area on the left two quadrants in Figure 6a). The impact of the head mesityl group in the right zone is less relevant, since it has to compete with the methylidene group for space. Nevertheless, the broad pale yellow area at 1.00−1.25 Å indicates that the mesityl ring is able to impart a noticeable steric pressure on the methylidene, particularly through the ipso and ortho C atoms (see the pale green imprints of these atoms in Figure 6a). The *o*-methyl groups of the mesityl ring have a small impact at the borders of the coordination sphere.

Quite interesting is the comparison between the SIMes and the SIPr in **7** and **8** (see Figure 6a,b). The bulkier ortho *i*-Pr groups of the head N substituent have a much stronger influence at the border of the coordination sphere (see the pale blue areas). To relieve the steric interaction between these groups and the halide atoms, the SIPr ligand is slightly pushed away. Consequently, the steric pressure on the central zone, where the Ru−methylidene bond is placed, is less encumbered by the SIPr rather than the SIMes ligand. This is clearly indicated by the absence of the pale green spots corresponding to the ortho C atoms of the ring in Figure 6b. In short, despite the similar $\%V_{Bur}$ values the two ligands shape remarkably different reactive pockets: quite flat and with a constant pressure for the SIMes ligand and vault-shaped with higher steric pressure at the border for the SIPr ligand. These differences, which cannot be captured by the simple $\%V_{Bur}$ descriptor, since it measures an average property, could contribute to the remarkable catalytic differences exhibited by the corresponding complexes.

Focusing on the *o*-tolyl NHC of **11**, small differences with respect to the SIMes of **7** also emerge. First, the space available on the top left tail quadrant, which corresponds to the unsubstituted side of the *o*-tolyl ring, is more hindered than the bottom left quadrant, which corresponds to the substituted side of the ring. Further, the top left quadrant is also more hindered that the analogous quadrant in the SIMes of **7** (see the deep violet area in Figure 6c). Similar asymmetry can be appreciated in the right head quadrants, and again the top quadrant is more buried with the imprint of the ortho C atom visible, whereas in the bottom quadrant, which corresponds to the substituted side of the *o*-tolyl ring, there is no trace of both the ortho C atom and its Me substituent.

Moving to the asymmetric NHC of **13**, the peculiar folding and the asymmetry of the catalyst can be appreciated in full. The steric map is asymmetric both in the tail (left) and head (right) quadrants. In both cases the less encumbered quadrants are those occupied by the *i*-Pr-substituted side of the N substituents. The unsubstituted side of the N substituent in the tail quadrants has an imprint similar to that of the *o*-tolyl ring in **11** (compare the similar purple areas in Figure 6c,d), whereas in the head quadrants the asymmetric NHC of **13** has a much greater impact (note the large green spot corresponding to the ortho C atom in the top right quadrant of Figure 6d). This clearly indicates that a substrate will prefer to coordinate to the Ru center (trans to the NHC) in such a way that bulkiness is placed in the *i*-Pr quadrants. This analysis supports the mechanism we proposed to rationalize the stereoselectivity in the desymmetrization of achiral trienes by **13**.[50]

Finally, it is interesting to note that the *o*-tolyl NHC in **11** presents a roughly C_s-symmetric map, with the two bottom quadrants more hindered, whereas the asymmetric NHC in **13** presents a roughly C_2-symmetric map, with the top left and bottom right quadrants more hindered. This can be qualitatively related to the rather good ability of the *o*-tolyl system to form cis olefins and supports our explanation of the higher enantiomeric excesses observed experimentally in the asymmetric ring closing metathesis of *E* olefins relative to the *Z* isomer.[48,50]

Analysis of Free NHCs. In this last section we discuss some features of free NHCs. We start with the energy profile around one of the ϕ angles for some of the most typical and uncoordinated NHCs ligands (see Figure 7). The NHCs have been chosen in order to exploit the effect of *o*-Me substituents and the nature of the NHC ring (saturated or unsaturated). The first result is that the two NHCs with phenyl N substituents prefer a planar geometry with the phenyl ring coplanar with the NHC ring (see the minima at $\phi = 0$ and 180° for the IPh

(78) Tolman, C. A. *Chem. Rev.* **1977**, *77*, 313.

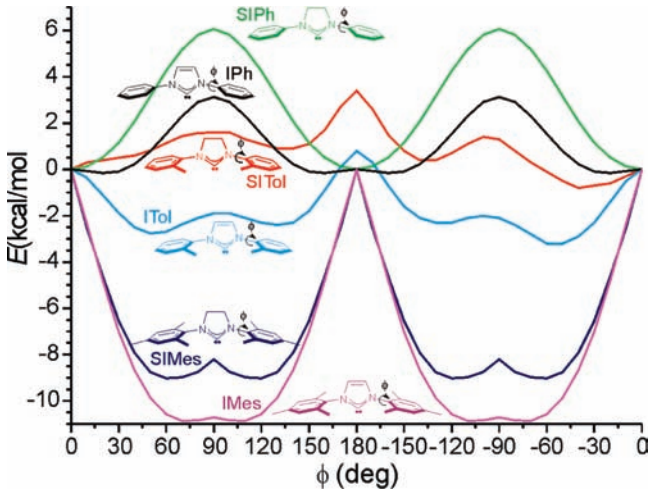

Figure 7. Energy profile around the ϕ angle in selected free NHCs.

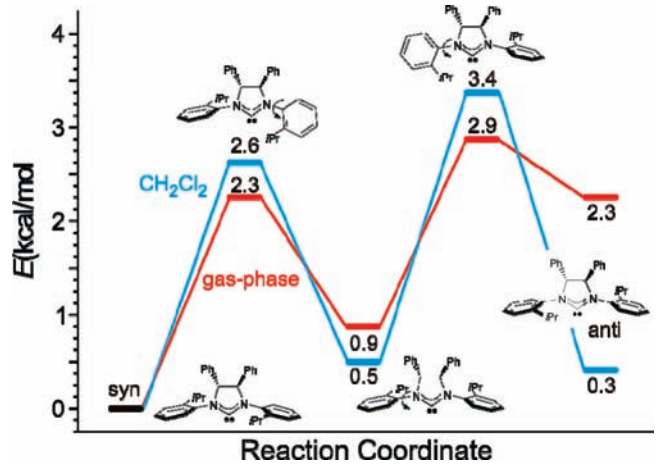

Figure 8. Isomerization pathway connecting the syn and the anti isomers of the NHC ligand of **13**.

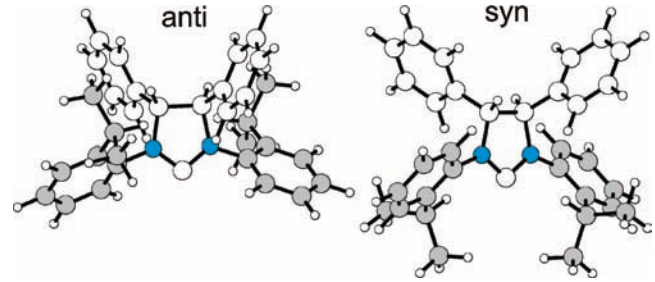

Figure 9. Optimized structure of the anti and syn isomers of the NHC of **13**.

and SIPh curves in Figure 7). The geometries with the phenyl ring almost perpendicular to the NHC ring are roughly 3 and 6 kcal/mol higher in energy for IPh and SIPh, respectively (see the maxima at $\phi = 90$ and $-90°$). Of course, the planar geometry is destabilized by steric repulsion between the NHC and the phenyl rings, but this destabilization is more than compensated by conjugation of the high-energy π orbitals of the NHC ring with the aromatic ring of the N substituents. The balance between these two effects rationalizes the various systems. Indeed, the presence of a single *o*-Me group introduces additional steric destabilization to the planar geometry, so that the energy curves of SITol and ITol are flatter and, in the case of ITol, the in-plane geometry is not the most stable. Finally, SIMes and IMes prefer a geometry with the mesityl rings almost perpendicular to the NHC ring (see the double shallow minima around $\phi = 90$ and $-90°$ in their curves in Figure 7).

The curves corresponding to saturated imidazoline NHCs are roughly 2−3 kcal/mol higher than those of the analogous unsaturated imidazole NHCs around $\phi = 90$ and $-90°$. This increased preference for the planar geometry in the case of the saturated NHCs can be ascribed to the different π orbital schemes between saturated and unsaturated NHCs. In the latter class the π orbitals of the N−C−N moiety are already stabilized by conjugation with the π orbitals of the unsaturated C4═C5 bond, whereas in the former class they are not. Incidentally, the different nature of the NHC skeleton has been also related to the higher tendency of saturated NHCs to dimerize.[47]

Finally, we explored the behavior of the asymmetric NHC ligand of **13** that can exist in the two limit isomers with the *i*-Pr groups away (anti) from the nearby Ph groups, as in the X-ray structure, or with the both the *i*-Pr groups on the same side (syn) of the Ph groups. Surprisingly, the syn isomer is more stable than the anti isomer both in the gas phase and in CH_2Cl_2, by 2.3 and 0.3 kcal/mol, respectively. We thus explored the isomerization pathway connecting them (see Figure 8).

The barriers separating the syn and anti isomers are roughly 3 kcal/mol, which indicates a rapid equilibrium between the two isomers, and the small preference for the syn isomer indicates that both isomers are abundantly present in solution. The slightly higher stability of the syn isomer can be easily rationalized by visual inspection of the structures reported in Figure 9. In both isomers the Ph rings on the NHC skeleton push the nearby side of the aromatic ring of the N substituent toward the carbenic C atom. In the anti isomer this corresponds to folding the *i*-Pr substituents toward the NHC backbone, while in the syn isomer the *i*-Pr groups are folded in a unhindered region, which corresponds to reduced steric stress in the syn isomer.

However, after complexation to the Ru center the syn isomer of **13** is 7.2 kcal/mol higher in energy than the anti isomer **13** of Chart 2, due to steric clashes of the folded-down *i*-Pr groups and the Cl ligand. These steric clashes can either prevent coordination of the metal to the syn isomer or can be considered as the driving force promoting isomerization of the syn isomer of complex **13** to the more stable anti isomer through rotation around the N−substituent bonds.

Conclusions

We have presented here a detailed static and dynamic characterization of a large set of NHC ligands in Ru complexes. Our analysis indicates that the nature of the N substituent can result in extremely different flexibilities of the Ru complexes. In almost all the cases the N substituent trans to the Ru−ylidene bond is severely folded in such a way that it protects the vacant coordination position at the Ru center, while somewhat limited flexibility is associated with the N substituent on the side of the Ru−ylidene bond. The phenyl N substituent can rotate almost freely, whereas rotation of the mesityl (or greater) N substituents is quite restricted. Results for the *o*-tolyl N-substituent indicate that one single ortho group on the N substituent is already enough to restrict flexibility remarkably. Two phenyl substituents on the C4−C5 bond are not enough to freeze phenyl N substituents, while four methyl substituents

do freeze them. In agreement with previous results, NHCs with a single ortho substituent, either a simple Me or a bulkier *i*-Pr, have a preferential folding that bends the unsubstituted side of the ring toward the halide−Ru−halide plane.

Analysis of the dynamics trajectories in terms of $\%V_{Bur}$ indicated that the real bulkiness of these systems at work can be somewhat modulated. The increased flexibility, which cannot be captured by static experimental or theoretical approaches such as X-ray or geometry optimizations, is instead fully captured and for the first time evidenced by our dynamics approach. In short, our results indicate that the flexibility around the N substituent bond is a key feature, so far underestimated, that allows NHCs to modulate their encumbrance around the metal in order to make room for bulky substrates.

Analysis of the $\%V_{Bur}$ values of the optimized structures in terms of steric maps illuminated the real impact of the NHC ligands in the first coordination sphere of the metal, which is the place where catalysis occurs. The comparative maps of the systems with mesityl and 2,6-diisopropylbenzene N substituents indicated that they shape rather different reactive pockets: rather flat with a constant pressure on the halide−Ru−halide plane in the former and vault-shaped with higher pressure on the side and lower pressure on the middle in the latter. As concerns the NHCs with an *o*-tolyl or an *o*-isopropyl group on the N substituent, the steric maps quantify the higher impact of the unsubstituted side of the ligand in the first coordination sphere of the metal and evidence the overall C_s- and C_2-symmetric reactive pockets of the corresponding complexes. We believe that a detailed characterization of the differently shaped reactive pockets is a further conceptual tool that can be used to rationalize the experimentally different performances of catalysts bearing these ligands or to devise new applications.

Finally, the Ru complexes we have investigated are relevant as (pre)catalysts for olefin metathesis. However, we believe that the emerged behavior can be easily extended to NHC ligands in almost any NHC-TM complex, with a particular emphasis on those able to promote catalytic activity for a broad spectrum of different applications. Indeed, our results indicate that some of the fundamental differences between various NHCs can be related to the intrinsic properties of NHC ligands.

Acknowledgment. We thank Dr. R. Rousseau, Pacific Northwest National Laboratory, for providing us the Ru pseudopotential and basis set for the CP2K simulations. We also thank one of the reviewers for useful suggestions. The research leading to these results has received funding from the European Community's Seventh Framework Programme (FP7/2007−2013) under grant agreement No. CP-FP 211468-2 EUMET. We thank BSC (Altamira projects QCM-2009-1-0006 and QCM-2009-2-0003) for access to remarkable computational resources and the HPC team of Enea (www.enea.it) for using the ENEA-GRID and the HPC facilities CRESCO (www.cresco.enea.it) in Portici, Italy. A.P. thanks the Generalitat de Catalunya for a Beatriu de Pinós postdoctoral contract.

Supporting Information Available: Text, figures, and tables giving a complete authors list for ref 55, Cartesian coordinates and energies, in hartree, of all the systems reported in Table 1, average values and standard deviations of the ϕ_1 and ϕ_2 angles, and convergence tests of the MD simulations and MPG movies giving MD simulations of systems **7**, **11** and **13**. This material is available free of charge via the Internet at http://pubs.acs.org.

JA909441X